A peptide pair coordinates regular ovule initiation patterns with seed number and fruit size

Nozomi Kawamoto[1,2], Dunia Pino Del Carpio[1,3], Alexander Hofmann[4], Yoko Mizuta[5,6], Daisuke Kurihara[6,7], Tetsuya Higashiyama[6], Naoyuki Uchida[6], Keiko U. Torii[6,8,9], Lucia Colombo[10], Georg Groth[2,3], and Rüdiger Simon[1,2*]

[1]Institute for Developmental Genetics, Heinrich-Heine University Düsseldorf, University Street 1, D-40225 Düsseldorf, Germany

[2]Cluster of Excellence on Plant Sciences (CEPLAS)

[3]Agriculture Research division, Agriculture Victoria, Australia

[4]Institute of Biochemical Plant Physiology, Heinrich-Heine University Düsseldorf, University Street 1, D-40225 Düsseldorf, Germany

[5]Institute for Advanced Research (IAR), Nagoya University, Furo-cho, Chikusa-ku, Nagoya, Aichi 464-8601, Japan

[6]Institute of Transformative Bio-Molecules (ITbM), Nagoya University, Furo-cho,

Chikusa-ku, Nagoya, Aichi 464-8601, Japan

[7]JST, PRESTO, Furo-cho, Chikusa-ku, Nagoya, Aichi 464-8601, Japan

[8]Department of Biology, University of Washington, Seattle, WA, 98195 USA

[9]Howard Hughes Medical Institute and Department of Molecular Biosciences, University of Texas at Austin, Austin, TX, 78712 USA

[10]Universita degli studi di Milano, Italy

*Corresponding author: Rüdiger Simon, ruediger.simon@hhu.de

Abstract

Ovule development in *Arabidopsis thaliana* involves pattern formation which ensures that ovules are regularly arranged in the pistils to reduce competition for nutrients and space. Mechanisms underlying pattern formation in plants, such as phyllotaxis, flower morphogenesis or lateral root initiation, have been extensively studied, and genes controlling the initiation of ovules have been identified. However, how a regular spacing of ovules is achieved is not known. Using natural variation analysis combined with quantitative trait locus analysis, we found that the spacing of ovules in the developing

fruits is controlled by two secreted peptides, EPFL2 and EPFL9 (also known as Stomagen), and their receptors from the ERECTA (ER) family that act from the carpel wall and the placental tissue. We found that a signalling pathway controlled by EPFL9 acting from the carpel wall through the LRR-receptor kinases ER, ERL1 and ERL2 promotes fruit growth. Regular spacing of ovules depends on EPFL2 expression in the carpel wall and in the inter-ovule spaces, where it acts through ERL1 and ERL2. Loss of EPFL2 signalling results in shorter fruits and irregular spacing of ovules or even ovule twinning. The EPFL2 expression pattern between ovules is under negative-feedback regulation by auxin, which accumulates in the arising ovule primordia. We propose that the auxin-EPFL2 signalling module evolved to control the initiation and regular, equidistant spacing of ovule primordia, which serves to minimise competition between developing seeds. Together, EPFL2 and EPFL9 coordinate ovule patterning and thereby seed number with fruit growth through a set of shared receptors.

Introduction

Plants have evolved diverse strategies to maximise their reproductive success, which

enables them to transfer genetic resources to subsequent generations. To produce floral organs at an appropriate time, plants integrate various environmental cues to induce flowering[1,2]. When this process is triggered in *Arabidopsis thaliana*, each flower produces four sepals, four petals, six stamens and one pistil which originates from the fusion of two carpels. The ovules, which contain the egg cells, reside in the pistil and are derived from another meristematic tissue within the pistil termed placenta[2,3], where they are almost simultaneously initiated in two parallel rows within each carpel. The number of ovules per flower determines the maximum number of seeds that a single flower can generate. At the transition from flower developmental stage 8 to 9 as defined by Smyth et al.[4], ovules are initiated from the placenta with regular 2 to 4 cell intervals. This regularity enables plants to reduce competition between adjacent ovules or the developing seeds after fertilization; disruption of this regular pattern could result in the formation of small or large, or closely juxtaposed ovules, which would bias reproductive success depending on random positional effects. During further growth, the pistil forms a silique that encloses the developing seeds until they reach maturity and are shed. Thus, the overall size of the silique places a natural constraint on the number of seeds that can be formed,

their final size, or both, and silique growth needs to be tightly coordinated with the ovule initiation process. Indeed, final fruit length is normally well correlated with the number of seeds grown within it[5]. However, how this coordination is achieved, and how ovules are initiated strictly at very regular intervals remains to be investigated.

Successful ovule formation is by itself a prerequisite for seed production and has therefore attracted widespread research interest, so that mechanistically, the process of ovule primordia formation is at least partially understood and the functions of key regulatory genes have been identified[2]. Ovule primordia originate from periclinal divisions in subepidermal cell layers of the placenta, and their formation requires the coordinated activity of auxin and cytokinin signalling pathways. Here, PIN1 acts as the main auxin transporter, and *pin1-5* mutants develop pistils with a reduced ovule number[6]. The expression of *PIN1* is further modulated by cytokinin. An increase in cytokinin levels due to loss of cytokinin degrading enzymes causes an increase in ovule number per flower, possibly by upregulation of PIN1 levels[7]. Other phytohormones involved are Gibberellins (GAs) and Brassinolide (BR), which act antagonistically to restrict (GA) or promote (BR) ovule formation via regulation of cytokinin signalling[8,9]. In response to

auxin, the transcription factor MONOPTEROS/AUXIN RESPONSE FACTOR5 (MP/ARF5) is activated and regulates the expression of the transcription factors AINTEGUMENTA (ANT), CUP SHAPED COTYLEDON1 (CUC1) and CUC2 in ovule primordia and the boundary domains between ovules, respectively[10]. A knockdown of *CUC1* expression in *cuc2* or *cuc2;ant* mutant backgrounds reduces ovule numbers, whereas *cuc2;cuc3* double mutants give rise to fused ovules, indicating that the generation of interorgan boundaries depends on partially overlapping CUC functions. CUC1 and CUC2 affect *PIN1* expression via control of cytokinin inactivating enzymes[7]. Overall, the process of ovule formation strongly resembles that of other lateral organs, where initials are first defined by local auxin accumulation[10]. The distance between ovule primordia determines ultimately the total number of seeds that can be generated on a single flower, if silique length is constant. A recent genome wide association study identified *NEW ENHANCER OF ROOT DWARFISM1* (*NERD1*) as a positive regulator of ovule number, however, the *nerd1* mutants generated drastically shortened siliques, suggesting that *NERD1* does not play a specific role in controlling the distance between arising ovules[11]. Alonso-Blanco and colleagues previously proposed the *ERECTA* (*ER*)

97 locus of Arabidopsis to be a major determinant of several life history traits, among them
98 fruit size and ovule number per flower[5]. The *er* mutants are characterised by a
99 short-fruit phenotype and a compact shoot architecture in the Landsberg background[12].
100 The *ER* gene encodes a leucine rich repeat (LRR) receptor kinase which regulates pattern
101 formation in multiple developmental pathways, including stomata development, vascular
102 architecture and leaf margin serration[13]; the related ER-family genes *ERECTA-LIKE1*
103 (*ERL1*) and *ERL2* contribute partially overlapping functions with ER[14–17]. Ligands for
104 ER-family receptors belong to the evolutionary conserved EPIDERMAL PATTERNING
105 FACTOR (EPF)/EPF-LIKE (EPFL)-family of cysteine-rich secreted peptides, with 11
106 members in Arabidopsis[18]. Some EPF/EPFL peptides act antagonistically in stomata
107 development by competing for interaction with the receptor complex, and consequently
108 trigger different signalling readouts in the stomata lineage[18–26]. For example, while EPF2
109 activates the MAPK cascade upon binding to the ER/ERL1/TMM receptor complex to
110 restrict entry of epidermal cells into the stomatal lineage, EPFL9/STOMAGEN competes
111 for binding and interacts preferentially with ER/ERL1[25]. Because EPFL9 binding does
112 not induce MAPK activation, SPCH is not degraded, resulting in the production of

113 supernumerous stomata[27,28]. Beyond epidermal cell specification, EPFL2 was found to
114 interact with ER, ERL1 and ERL2 to promote leaf margin tooth growth via regulation of
115 auxin responses[17].
116 We started to investigate the underlying mechanisms of regular ovule initiation by asking
117 whether the spacing of ovules is largely genetically or environmentally controlled. A
118 natural variation analysis combined with QTL analysis of candidate lines first identified
119 *ER* and *EPFL2* as key loci that control the spacing of ovules in the developing fruit.
120 Detailed genetic and gene function analyses further revealed that at least two separate
121 pathways involving members of the ER and EPF families control regular spacing of
122 ovules, together with fruit size. We propose that the tight coupling of fruit growth with
123 ovule initiation at regularly spaced intervals depends on the negative feedback regulation
124 between EPFL2 and auxin. The output of this patterning module would safeguard a low
125 variance between ovules as a conservative bet hedging approach.
126
127 **Results**
128 **ER regulates the density of ovules**

Because key genes controlling ovule formation such as *PIN1*, *MP* or *CUC1* act in multiple processes of organogenesis in plants, their interactions might be hardwired, and classical mutant screens might not deliver insights into the regulation of ovule density patterning itself. We therefore first resorted to study the range of variation in ovule density that can be observed between natural accessions of Arabidopsis. We grew the accessions at two different temperatures as a proxy to further access environmental control of this patterning process. For 96 accessions, we measured fruit length and the number of seeds including unfertilized ovules (= total number of ovules) per fruit in stage 17 flowers (all stages according to Smyth et al.,[4]), and calculated total ovule density as a derived trait (total number of ovules per mm fruit length). The total ovule density strongly varied between accessions and temperatures, ranging from 2.37 to 6.36 (N/mm) (Figure S1). Our natural variation analysis revealed several accessions with a characteristic ovule-density phenotype (Figure 1A, B), which was only mildly affected by temperature. Hence, we sought regulators by applying QTL analysis to L. *er* x Cvi-0 recombinant inbred lines (RILs), since Cvi-0 has long fruits and a low ovule density, whereas L. *er* carries shorter fruits with a high ovule density (Figure 1A, B). QTL analysis allowed us to

find a significant peak on chromosome 2 (Figure 1C). Among many loci in this chromosomal region, the *ER* locus seemed to be the most influential candidate. The accessions Landsberg *erecta* (L. *er*) and Vancouver-0 (Van-0) were characterized by shorter fruit and a higher ovule density compared to other accessions (Figure 1B, Figure S1). The L. *er* and Van-0 accessions both carry mutations in the *ER* locus and are known *er* loss-of-function mutants[29,30]. In addition to these two accessions, Hiroshima-1 (Hir-1) is also known as an *er* loss-of-function mutant[29,30]. To test the functional importance of *ER* gene in the control of ovule density, we assessed fruit phenotypes in the *er* mutant lines complemented with a wildtype copy of the *ER* locus[29–31]. The short fruit and high ovule density phenotypes in all three accessions were complemented by functional *ER* genomic DNA from Columbia (Col) (Figure S2). Furthermore, the *er-105* mutant in a Col background showed a similar phenotype to the L.*er*, Van-0 and Hir-1 accessions (Figure 2A, Figure S2, S3). These results clearly indicate that *ER* is necessary for the control of ovule density, and that ER acts similarly in different genetic backgrounds.

ERL1 and ERL2 antagonistically function to ER in the regulation of ovule density

Two *ER* paralogous genes, *ERL1* and *ERL2* have overlapping, yet distinct functions with *ER* in the regulation of plant architecture[11]. To investigate the potential role of *ERL1* and *ERL2*, we analyzed *ER*-family receptor mutants in a Col background[15]. Although *erl1-2* and *erl2-1* single mutants did not display an obvious phenotype, the *erl1-2*; *erl2-1* double mutant developed shorter fruits and lower ovule density than the wild-type (Figure 2A, Figure S3). This is in contrast to *er*-mutants, which carried also shorter fruits, but with a higher ovule density than wild type. When combined with *er-105*, either *erl1-2* or *erl2-1* further enhanced the fruit length phenotype and displayed reduced total ovule number, but surprisingly an even higher ovule density (Figure 2A, Figure S3). Since *er-105; erl1-2; erl2-1* triple mutants are very dwarfed and do not produce proper flower organs[32] (Figure 2B, C), it was impossible to analyze their fruit or ovule density phenotype. However, our results indicate that *ERL1* and *ERL2* function jointly with *ER* to promote fruit growth, whereas two separable *ERL1/2* and *ER* dependent pathways antagonistically regulate ovule density.

EPFL9 is a ligand for ER family receptors that controls fruit elongation

177 Our genetic analysis suggested that two independent pathways antagonistically control
178 ovule density- *ER* functions to decrease ovule density whereas *ERL1* with *ERL2* increase
179 ovule density. This suggests that unknown ligands, binding to ER-family receptors, may
180 be involved in ovule density control. Previous work identified EPF/EPFL family peptides
181 as ligands of ER-family receptors that control a variety of biological
182 processes[19,20,35,21–26,33,34]. We found that within the *EPF*/*EPFL* family, *EPFL9* is
183 expressed in developing fruits by searching a public expression database. EPFL9 has a
184 unique function in stomatal patterning[21–23], since all other EPF/EPFL peptides except
185 EPFL9 reduce the number of stomata by activating a downstream MAPK cascade via ER
186 family receptors[17,18,34,35,19–26]. EPFL9 also interacts with ER-family receptors, but its
187 binding does not activate a MAPK cascade[25], thus acting in an antagonistic manner to the
188 other EPF/EPFL peptides. We then hypothesized that EPFL9 might function as a ligand
189 for the control of ovule density. Since an EPFL9 mutant was not available, we analyzed
190 STOMAGEN RNAi plants[21] and found a clear reduction of fruit length and a higher
191 ovule density than in wild-type plants (Figure 3A, Figure S4). Together, the phenotype
192 was weaker than that of *er-105* mutants (Figure 2A, Figure S3). Our result suggests that

193 EPFL9 functions through ER family receptors to promote fruit growth, possibly in
194 conjunction with other related ligands.
195
196 **EPFL2 as a ligand for ER-family receptors in ovule spacing**
197 As we described above, EPFL9 functions as a ligand of ER in the stomata pathway. We
198 sought further regulators of ovule density by re-analyzing our QTL data set using the ER
199 marker on chromosome 2 as a cofactor. Cofactor analysis allowed us to improve the
200 detection power and decrease a type II error (false negative)[36]. QTL analysis revealed
201 additional contributing regions on chromosome 4 and 5 for the control of seed density
202 (Figure 1D). Among the candidate loci, we focused on *EPFL2* (At4G37810) on
203 chromosome 4, which acts with ER-family receptors to control leaf serration[17]. The
204 *epfl2-1* mutation in the L.*er* background caused, compared to L.*er*, a minor fruit
205 shortening but a major reduction in ovule number, so that the resulting ovule density was
206 lowered (Figure S5). When *ER* genomic DNA was introduced into the *epfl2* L.*er*
207 accession (L.*er ER*+), the phenotype was still characterized by short fruit length, a low
208 ovule number and a low ovule density (Figure 4A, Figure S5), indicating that *EPFL2* acts

209 independently of *ER*. Overall, the *epfl2-1* phenotype closely resembled that of *erl1-2;*
210 *erl2-1* double mutants (Figure 2A, Figure 4A, Figure S3, Figure S5), suggesting that
211 ERL1 and ERL2, and not ER, are the key receptors for perception of EPFL2. Since *erl1*
212 and *erl2* mutants are in the Col accession, we generated the novel *epfl2-2* mutant allele in
213 the same genetic background using CRISPR/Cas9 for further genetic analysis. We then
214 crossed *epfl2-2* with *erl1-2; erl2-1* to generate *epfl2-2; erl1-2; erl2-1*, and with *er-105* to
215 generate *epfl2-2; er-105*. The *epfl2-2; erl1-2; erl2-1* triple mutant showed a similar
216 phenotype to the parental lines *epfl2-2* and *erl1-2; erl2-1* (Figure 4B, Figure S8).
217 Furthermore, *epfl2-2; er-105* displayed an additive phenotype, as observed in L. *er;*
218 *epfl2-1* (Figure 4B, Figure S5, Figure S8). We conclude that EPFL2 mainly functions
219 with ERL1 and ERL2, and not with ER.
220
221 **Loss of *EPFL2* causes irregular patterning and twinning of ovules**
222 We observed abnormal ovules and seeds in both *epfl2* mutants. In some cases (0.27%),
223 two ovules were initiated and developed from a single funiculus (Figure 5A, B).
224 Although EPFL2 functions in the ERL1 and ERL2 pathway, this twin-ovule phenotype

was not observed in *erl1-2; erl2-1* plants, but in the *epfl2-2; erl1-2; erl2-1* and *epfl2-2; er-105*, indicating that EPFL2 can act also independently of ER-family receptors. In *epfl2* mutant plants, neighboring cells on the placenta appear to acquire ovule identity and differentiate into ovules, resulting in twins. In order to visualize early ovule initiation patterns, we introduced *pDORNRÖSCHEN(DRN)::erGFP* as a marker for the earliest stages of ovule initiation. During embryogenesis, *MP* activates expression of the auxin-responsive transcription factor *DRN* in the tip of cotyledons[37,38]. The semi-quantitative auxin reporter R2D2[39] revealed that auxin maxima are established at the tip of ovule primordia coinciding with *DRN* expression (Figure 5C-E), indicating that *DRN* expression also reflects auxin distribution[37,38], and thus can serve as marker to visualize ovule initiation patterns. Before ovule initiation, *DRN* was ubiquitously expressed in the placenta (Figure 5F, G), but when placental cells acquire ovule identity, *DRN* expression becomes confined to the ovule initial cells (Figure 5H, I). In wild-type plants, the ovules initiated with 2 to 4 cells intervals (Figure 5J, L). In *epfl2-2* mutants, *DRN* was expressed in a much broader pattern (Figure 5K) and *DRN* expression domains appeared less regularly spaced (Figure 5K, L). We quantified the spacing by counting the

241 number of cells between adjacent ovule primordia. In the wildtype, we found on average
242 2.97 cells between two ovule initial cells, and these average values were slightly
243 increased for the *epfl2* mutant lines (3.10 cells). Importantly, cell numbers in *epfl2* varied
244 from 1 to 6 cells, whereas the wild-type displayed a very regular ovule spacing with cell
245 numbers ranging between 2 to 4 (Figure 5L). We conclude that EPFL2 serves the
246 initiation of ovules at regularly spaced intervals.
247
248 **ER-family receptors are coexpressed with EPFL2 and EPFL9 in pistils**
249 From our genetic analysis, we concluded that two major pathways control ovule
250 patterning. One is the EPFL9/ER pathway that mainly controls fruit growth, the other is
251 the EPFL2/ERL1/ERL2 pathway which has a major impact on ovule density via
252 regulating ovule initiation patterns, and also weakly contributes to fruit growth. We next
253 analyzed the expression profiles of *ER*, *ERL1*, *ERL2*, *EPFL9* and *EPFL2*. ER-family
254 receptors were previously shown to be expressed in different parts of the pistil[15,40]. For
255 the analysis of ER, ERL1 and ERL2, we used translational fusion lines with YFP as a
256 reporter[24,41] and for EPFL9 and EPFL2 we generated transcriptional reporter lines using

257 EGFP and TdTomato as fluorescent tags with Histone H2B[17,21]. To visualize the
258 expression patterns, we combined tissue clearing[42] and confocal microscopy. In stage 8
259 flowers, ER was broadly expressed in various organs including carpels (Figure 2D),
260 consistent with previous observations[43]. In the pistils, ER was mainly expressed in the
261 valve (Figure 2E)[43], but signal was also weakly detected in ovule primordia and
262 inter-ovule spaces (Figure 2E). ERL1 expression was not detected in the carpels at early
263 stages of development (Figure 2F). ERL2 was expressed in the carpels including the
264 placenta before ovule primordia became apparent (Figure 2H). When ovule primordia
265 were initiated, the expression of ERL1 and ERL2 was detected in inter-ovule spaces and
266 the ovule primordia (Figure 2G, I). The signal of ERL2 was strongly visible at the
267 boundary and the tip of ovule primordia which will develop into the nucellus, the outer
268 and the inner integuments, but signal was weaker in the basal domian of ovule primordia
269 (Figure 2I). Compared to ERL2, ERL1 signals were weaker and somehow patchy (Figure
270 2G). ERL1 and ERL2 were only weakly expressed in valves (Figure 2G, I). As expected
271 from the STOMAGEN RNAi phenotype, EPFL9 was exclusively expressed in the inner
272 cell layers of the valves (Figure 3D, E) from stage 8 onwards (Figure 3B, C) but lacking at

the valve margin and the replum (Figure 3E). The expession patterns are consistent with EPFL9 acting as a short range signal that controls fruit growth via ER. In contrast to EPFL9, EPFL2 expression was detected in the placenta (Figure 4E, F), and importantly, once the ovule primordia were initiated, confined to the inter-ovule spaces (Figure 4E, F, G). In transverse sections, EPFL2 expression was also visible in the valve, around the valve margin and the replum (Figure 4F). However, expression was not noted in carpels of stage 8 flowers (Figure 4C, D). As previously reported[44], EPFL2 seems to be preferentially expressed at the boundary between ovules.

Altered expression of EPFL2 affects the ovule initiation pattern

The *DRN* expression profile in the placenta is largely complementary to that of *EPFL2* (Figure 4C, D, E, F, G, 5F, G, H, I). To further test the importance of *EPFL2* in the pattern of ovule initiation, we characterized the transgenic plants which misexpress *EPFL2* from the *DRN* promoter (Figure 5F, G, H, I). When *EPFL2* misexpression was driven by the *DRN* promoter in a wild-type background (*pDRN::EPFL2)*, the resulting transgenic plants carried fruit with a length similar to the non-transgenic siblings (Figure S9), but

showed a significantly reduced ovule number and ovule density (Figure 5M, Figure S9). This indicated that EPFL2 cannot promote fruit growth from the placenta domain, and that a regular and interspersed expression of EPFL2 is required for proper spacing of ovule initiation.

Quantitative analysis reveals interactions between peptides and receptors

Our genetic analysis indicates that EPFL2 acts preferentially via ERL1 and ERL2; however, earlier co-immunoprecipitation experiments in *Nicotiana benthamiana* have shown that EPFL2 can physically associate with all ER-family receptors *in vivo*[17]. Because EPF/EPFL peptides may bind to ER-family receptors with different affinities[45], we investigated interaction properties between ER-family receptors and their ligands EPFL9 and EPFL2 *in vitro*. Recombinant peptides and the extracellular domains of ER-family receptors were expressed in *E. coli* and purified. Because EPFL2 and EPFL9 are cysteine-rich and their final conformation is stabilized by the formation of specific disulfide bonds, the peptides were first affinity purified, refolded in refolding buffer, and separated from unfolded peptides by HPLC[24]. We then evaluated peptide bioactivity by

measuring their impact on stomatal density. As a control, six cysteine residues of EPFL2 were substituted to serine residues (EPFL2 (CS)), which should render the peptide less stable. As observed in transgenic EPFL2-overexpressing Arabidopsis lines[17,35], EPFL2 treatment reduced the number of stomata (Figure S11B, I), whereas EPFL9 had the opposite effect (Figure S11D, I). Furthermore, since TOO MANY MOUTH (TMM) is a stomatal lineage specific co-receptor protein[46] and not expressed at the carpel wall and the placenta (Figure S10), we also used *tmm-KO* plants. *tmm* knockout mutants were found to be sensitized for EPFL2 and responded more strongly (Figure S11F, I), which is consistent with previous studies[35,45]. These assays indicated that the purified peptides were functional. We then tested the direct interactions between the peptides and receptors using isothermal titration calorimetry (ITC). Both EPFL2 and EPFL9 bound to the extracellular domain of ER-family receptors, albeit with different affinities. EPFL2 showed a binding preference for ERL1 and ERL2 (Figure S12). EPFL9 bound to ER, ERL1 and ERL2 with similar affinities (Figure S12).

From our combined data, we propose that regular spacing of ovules at defined intervals is coordinated with fruit growth through the EPFL2/ERL1/ERL2 and EPFL9/ER signalling

321 pathways.

322

323 **Discussion**

324 In selfing species such as Arabidopsis, pollen availability is no longer a limiting factor for
325 fertilization, and the key determinant for seed production is now ovule number. The
326 total number of seeds that can be generated by an individual plant depends on the
327 available resources which can be invested into the formation of branches carrying
328 flowers.
329 Overall reproductive success then depends on the total number of flowers, and the
330 number of ovules that are being initiated in each individual flower. In the developing
331 Arabidopsis ovary, ovules are initiated from the placenta, and the total length of the pistil
332 at the time of ovule initiation restricts the maximum number of ovules that can be formed.
333 Not suprisingly, there is a general correlation between fruit length and overall seed
334 number, so that ecotypes that generate longer siliques also bear more seeds. The genetic
335 basis of ovule initiation and fruit growth has been studied in much detail, and a number of
336 key transcription factors and phytohormones have been investigated which control the

337 formation of ovules and fruit development. However, the fundamental patterning
338 mechanism that determines the spacing of ovule anlagen within the placenta remained
339 unexplored.

340 Organ initiation in plants generally requires auxin accummulation at discrete sites. Using
341 the auxin-regulated transcription factor DRN as a sensor for auxin signalling, we found
342 that an evenly distributed auxin signal in the developing placenta is resolved into a
343 regularly spaced pattern of founder cells of the young ovules. Importantly, this patterning
344 process is not a repetitive process and takes place in a structure with a finite size, which
345 clearly distinguishes it from other well studied patterning processes in plants, such as
346 phyllotaxis or stomatal patterning. We therefore carried out a natural variation analysis
347 and QTL analysis to identify genes responsible for ovule density, leading to the
348 identification of *ER* and *EPFL2*. Additionally, we found that the ER paralogs ERL1 and
349 ERL2, as well as the EPF/EPFL-family peptide EPFL9, also regulate ovule density. Our
350 genetic interaction studies and expression analysis showed that these two pathways
351 control ovule density in distinct ways. The EPFL9 pathway, acting from the carpel wall,
352 exclusively controls fruit elongation without affecting the ovule initiation pattern.

353 Reduction of ovule number observed in *er-105* seems to be an indirect consequence of the
354 smaller fruit size and the limited availability of space. The EPFL2 pathway also affects
355 fruit growth, but has a more pronounced impact on the patterning of ovule initial cells and
356 thus increases ovule density (Figure 6A, B).
357 We observed ovule twinning in *epfl2* mutant plants, which is caused by mis-patterning
358 during ovule initiation. Furthermore, ectopic expression of EPFL2 also caused ovule
359 patterning defects, which we interpret that EPFL2 is a dosage-sensitive regulator of ovule
360 initiation. Our genetic, biochemical and expression data further suggest that ERL1 and
361 ERL2 are the main receptors for EPFL2. Among these two, ERL2 has a major role as a
362 receptor for EPFL2 for two reasons: First, the *erl2-1* mutant enhanced the *er-105*
363 phenotype more severely than *erl1-2*, and second, ERL1 is expressed at lower levels than
364 ERL2 in the placenta. Ovule twinning was observed in *epfl2-2; erl1-2; erl2-1* as well as
365 *epfl2-2* mutants, but not in *erl1-2; erl2-1* mutants, suggesting that in the absence of ERL1
366 and ERL2, other receptors contribute to EPFL2-mediated ovule initiation. TMM is a
367 well-characterized co-receptor for ER-family receptors in stomata development, but
368 since TMM is not expressed in the pistil (Figure S10) [46], it is not likely to act here.

The transcriptional regulation of EPFL2 is so far unknown, but it is tempting to speculate that the transcription factors, CUC1, CUC2, and CUC3 are potential upstream regulators of *EPFL2* expression, because their expression profiles are similar to that of EPFL2 [10,47], and *CUC1 RNAi; cuc2* plants produce fewer ovules than wild-type plants [10]. Transcriptomic analysis revealed that some of EPFL family genes were downregulated in *CUC1 RNAi; cuc2* plants[7]. *cuc2-3; cuc3-105* mutants can carry twinned ovules [47], as seen in *epfl2*, and *EPFL2* expression under the control of the *CUC2* promoter was sufficient to restore the leaf margin serration phenotype of *epfl2* mutants [17].

Prior to ovule primordia initiation, *DRN* expression was uniformly observed at the placenta (Figure 5C). Since *DRN* is a direct target of MP [38], auxin seems to be signalling uniformly during early stages of placenta growth. However, once placenta cells adopt ovule identity, auxin maxima are established at the tip of ovule initials [2] (Figure 5C-E) and *DRN* expression is confined to these positions (Figure 5H). We propose that similar to the feedback mechanism that operates in leaf margin development [17], *EPFL2* restricts auxin accumulation to the developing ovule primordia, while auxin at the same time provides a feedback signal that supresses *EPFL2* expression (Figure 6C). This

auxin-*EPFL2* negative feedback loop provides an important new element to control precise and highly regular ovule spacing patterns, which safeguards equal nutrient access as a bet hedging strategy. With its additional function in promoting fruit growth due to expression in the carpel wall, *EPFL2* thus serves to integrate these two processes. Life history variations that necessitate trade-offs between seed number, seed size and fruit size could then act through differential expression of *EPFL2*.

Cultivated asian rice was selected for awnlessness to facilitate harvesting. One of the underlying causal mutation inactivates an *EPFL2*-orthologue, OsEPFL1, which also affects grain length and grain number, giving rise to more compact panicles with more seeds [48–50]. Although the underlying mechanism in rice is not yet understood, it highlights a role of *EPFL2*-genes as evolutionary conserved integrators of ovule initiation patterns, seed number, seed size and floral organ development [51].

Materials and Methods

Plant materials and growth conditions

For natural variation analysis, 96 *A. thaliana* ecotypes [52] were planted and grown in

401 continuous light at either 16˚C or 21˚C. After germination, the plants were vernalized for
402 6 weeks at 4˚C. For QTL analysis, 165 RILs [5] were planted and grown in continuous light
403 at 16˚C. For phenotypic and expression analysis, plants were grown under long-day
404 conditions (16-h photoperiod). The Van-0, Van-0 *ER*+, Hir-1, and Hir-1 *ER*+ accessions
405 were previously described [30]. The L. *er; epfl2-1* (CSHL_ET5721), L. *er; epfl2-1; ER*+,
406 and L. *er; ER*+ lines were previously described [17]. An *epfl2* mutant in the Columbia
407 accession was generated by CRISPR/Cas9. For this, we designed two single guide RNAs
408 targeting *epfl2* (Figure S6A) in one vector. We obtained five different *epfl2* mutant alleles
409 in the T2 generation (Figure S6B), all of which caused a smoother leaf margin phenotype
410 indicative of *epfl2*-mutants (Figure S6C) as previously reported [17]. For further analysis,
411 #36-45 which has a genomic deletion between the sgRNA1 and 2 target sites was selected.
412 Hereafter we refer to the original *epfl2* mutant in L. *er* (CSHL_ET5721) as *epfl2-1* and
413 our new allele #36-45 as *epfl2-2*. Consistent with our previous analysis using *epfl2-1*, we
414 found that *epfl2-2* phenocopies *epfl2-1* (Figure 4A, Figure S7), and that *epfl2-2* mutants
415 also resemble the *erl1-2; erl2-1* phenotype (Figure 2A and 4A). The *gER:YFP; er-105*,
416 *gERL1:YFP; erl1-2* and *gERL2:YFP* lines were previously described [24,41]. The *er-105*,

417 *erl1-2, erl2-1, er-105; erl1-2, er-105; erl2-1, erl1-2; erl2-1* lines were previously
418 described [15]. The STOMAGEN RNAi line was generated [21]. The *pDRN::GFP; Col* was
419 described [38]. The auxin semi-quantitative marker line R2D2 was developed in [39]. The
420 *epfl2-2* and *epfl2-3* lines were generated by CRISPR/Cas9 genome editing in this study,
421 and the *epfl2-2; er-105, epfl2-2; erl1-2; erl2-1* were generated by genetic crossing. We
422 also generated the following transgenic plant lines: *pEPFL2::H2B:TdTomato;* Col,
423 *pEPFL9::H2B:EGFP:3HA:His; Col, pDRN::EPFL2;* Col, and *pDRN::GFP; epfl2-2*.
424 Plants were transformed using *Agrobacterium tumefaciens* strain GV3101 or C58 pSOUP
425 via the floral dip method.
426
427 **QTL analysis**
428 For the RIL population, the final phenotype value for each line was calculated as the
429 average of all the replicates. The Genotype information from 243 markers in the Ler/Cvi
430 RIL map was collected from available published data [5]. QTL analysis was performed
431 within the R statistical software with the qtl package [53] using a Multiple QTL Mapping
432 (MQM) approach. In the MQM mapping approach, we used a forward stepwise approach

433 preselecting the ERECTA marker as a cofactor.

434

435 **Plasmid constructs**

436 The plasmids and primers used in this study are listed in Table S1. Vectors pFH1 and
437 pFH6 [54] along with the in-house vector pUB-Cas9-@EPFL2 were used for the knockout
438 of *EPFL2* with the CRISPR/Cas9 system. To generate the construct
439 pEPFL2::H2B:TdTomato, *EPFL2* promoter DNA was amplified by PCR from Col
440 genomic DNA and inserted at the HindIII and SmaI sites of pPZP211/35S using the
441 InFusion kit (Clontech) yielding the intermediate vector pPZP211/pEPFL2. The *H2B*
442 (At5g22880) gene was amplified from Col cDNA and was inserted into the SmaI and
443 SacI sites of pPZP211/pEPFL2 using the same method, yielding vectors
444 pPZP211/pEPFL2::H2B. Finally the TdTomato gene was amplified and inserted into the
445 SacI and SacII sites of pPZP211/pEPFL2::H2B to generate
446 pPZP211/pEPFL2::H2B:TdTomato. To generate the construct pEPFL2::EPFL2, the
447 *EPFL2* coding sequence was inserted into pPZP211/pEPFL2 at the BamHI and SacII
448 sites. To construct the pDRN::EPFL2 vector, the *DRN* promoter and terminator

449 sequences and the *EPFL2* coding sequence were amplified by PCR from Col genomic
450 DNA or cDNA and inserted into vectors pGGA000, pGGE000, and pGGC000
451 respectively. The pGGZ001, pGGA000-pDRN, pGGB002, pGGC000-EPFL2,
452 pGGD002, pGGE000-tDRN and pGGF007 DNA fragments were then assembled by
453 GreenGate cloning [55]. For pEPFL9:H2B-EGFP(or TdTomato):3HA:His, the *H2B* gene
454 was amplified as above and inserted into the SmaI and SacI sites of
455 pPZP211/35S:EGFP(or TdTomato)-3HA-His [56]. The plasmids were digested with XbaI
456 and EcoRI, and the H2B-EGFP (or TdTomato) 3HA-His:NosT fragments were
457 transferred to vector pPZP211. The *EPFL9* promoter was amplified from Col genomic
458 DNA and inserted into the vectors at the SalI and SmaI sites using the InFusion kit as
459 above. Codon optimized mature EPFL2 and mutated mature EPFL2 sequences were
460 synthesized (Thermo Fisher Scientific) and cloned into the SacII and XhoI sites of
461 pET41a. Mature EPFL9 was amplified from *Arabidopsis thaliana* Col cDNA and cloned
462 into pGEX4T1 by Gibson assembly (NEB). Ectodomains of ER (E25-R580), ERL1
463 (M26-R582), ERL2 (M28-R585) were amplified from *Arabidopsis thaliana* Col cDNA
464 and cloned into pETEV16 by Gibson assembly (NEB).

465

466 **Photography of leaves**

467 To characterize the leaf margin, the seventh leaf of each plant was photographed under a

468 Nikon SMZ25 stereomicroscope.

469

470 **Data visualization and statistical analysis**

471 R (version 3.5.1) was used for data visualization and statistical analysis. The following

472 statistical tests were used to calculate the corresponding p-values. A two-tailed Student's

473 t-test was used for pairwise comparisons, whereas Dunnett's test and Tukey-Kramer's test

474 were used to compare multiple sets of data to a control or all possible pairs, respectively.

475 F-test was used to compare two variations. In each case, a value of $p < 0.005$ was

476 considered significant.

477

478 **Tissue clearing and expression analysis**

479 Flowers and pistils were dissected under a standard dissection microscope. The samples

480 were fixed in freshly prepared 4% paraformaldehyde in PBS (pH 7.4) supplemented with

481 0.05% Silwet L-77 for 3–5 h under vacuum, followed by incubation in ClearSee as
482 previously described [41]. The tissues were then stained with Calcofluor White to
483 visualize the cell walls. The processed tissues were observed under a confocal
484 microscope (Carl Zeiss LSM780, Carl Zeiss LSM880 or Leica TCS SP8). For GFP, the
485 excitation wavelength was 488 nm and the signal was detected at 500–550 nm. For YFP,
486 the excitation wavelength was 514 nm and the signal was detected at 520–575 nm. For
487 TdTomato, the excitation wavelength was 561 nm and the signal was detected at 565–600
488 nm. For Calcofluor White, the excitation wavelength was 405 nm and the signal was
489 detected at 415–475 nm. These ranges were selected to avoid overlaps between the
490 signals.
491
492 **Peptide expression, purification and refolding and protein expression**
493 Mature EPFL2 (MEPFL2) and mutant mature EPFL2 (mMEPFL2; C60S, C65S, C68S,
494 C71S, C119S, C121S) were heterologously expressed in *E. coli* BL21 (DE3) as
495 GST-His-tagged fusion proteins. EPFL9 was expressed only as GST-fusion protein in *E.*
496 *coli* BL21. Peptides were purified via GST affinity chromatography by FPLC (Äkta

497 Prime Plus, GE Healthcare). The GST tag was proteolytically cleaved by TEV-protease
498 digestion. Peptides were separated from free GST and residual protease via reverse
499 phase-HPLC (Supelcosil, LC-18 HPLC column, 15x4.6 cm, 3µm particle size) under an
500 acetonitrile gradient (0-100% v/v) with 0.1%TFA (v/v). After vacuum assisted solvent
501 evaporation, peptide pellets were resolved in refolding buffer as previously described to
502 introduce proper disulfide bridges, which were indirectly verified by the stomata density
503 based bioactivity assay. Peptide identities and purities were confirmed by mass
504 spectrometry which revealed two additional amino acids (Gly-His) were attached at
505 N-terminus of each peptide, as results of the TEV-protease cleavage.
506 Receptor domains of ER (E25-R580), ERL1 (M26-R582), ERL2 (M28-R585) and TMM
507 (F24-G475) were heterologously expressed in *E. coli* BL21 (DE3) with an N-terminal
508 His-tag and TEV-protease target sequence. The expressed protein domains were purified
509 via Ni^{2+} affinity chromatography by FPLC (Äkta Prime Plus, GE Healthcare). The eluted
510 proteins were subjected to buffer change by PD10 desalting column into ITC-buffer (25
511 mM BisTris-HCl pH6.0, 150 mM NaCl, 50 mM L-arginine and 50 mM L-glutamic acid).
512

513 **Peptide bioassay**

514 Col and *tmm* knockout (*tmm-KO,* Salk_011958) seeds were sterilized and sown on
515 half-strength MS medium. Prior to germination, seeds were kept in the dark at 4˚C for 3
516 days, then transferred to continuous light at 22˚C for germination. One day after
517 germination, the seedlings were transferred to 1 ml half-strength MS liquid medium
518 supplemented with 5 µM of the appropriate peptide in 0.5 g/L MES-KOH (pH 5.7) and
519 were incubated as above for 5 days. At the end of the treatment period, the cotyledons
520 were stained with 1 µg/ml propidium iodide and observed under a Confocal microscope
521 (Carl Zeiss LSM710, Carl Zeiss LSM880 or Leica TCS SP8). For excitation, 561 nm
522 laser line was used and signal was collected between 565–650 nm. The MES-KOH buffer
523 (pH 5.7) without peptides was used for the mock treatment.

524

525 **ITC**

526 ITC-experiments were carried out in a MicroCal iTC200 (Malvern Instruments) at 25°C
527 with a sample cell of 280 µL and an injection syringe of 40 µL. Peptide pellets were
528 dissolved in ITC-buffer and peptide concentrations were assessed by FTIR with a

529 DirectDetect system (Merck). Protein concentrations of the receptor domains were
530 measured by absorption at 280 nm and calculated by their molar absorption coefficient at
531 280 nm. The molar coefficients for ER, ERL1 and ERL2 (42400, 41410, and 42400 M^{-1}
532 cm^{-1}, respectively) were calculated based on ExPASy ProtParam. Final protein and
533 peptide concentrations are as indicated. For each experiment 19 injections of 2 µL with a
534 spacing of 150s were performed.
535

536 **Acknowledgement**

537 We thank the Center for Advanced imaging (CAi) at the Heinrich-Heine University
538 Düsseldorf for support with microscopy. We are grateful for receiving Arabidopsis seeds
539 from the following colleagues: Martijn van Zanten (Van-0, Van-0 ER+, Hir-1, Hir-1
540 ER+), Wolfgang Werr (pDRN::GFP), Dolf Weijers (R2D2) , Dominique Bergmann
541 (gERL2:YFP), Ikuko Hara-Nishimura and Tomoo Shimada (STOMAGEN RNAi). This
542 work was supported by the DFG through the Cluster of Excellence on Plant Sciences
543 (CEPLAS, EXC1028).
544

545 ## References

546 1. Srikanth, A. & Schmid, M. Regulation of flowering time: All roads lead to Rome.
547 *Cell. Mol. Life Sci.* **68**, 2013–2037 (2011).

548 2. Cucinotta, M., Colombo, L. & Roig-Villanova, I. Ovule development, a new
549 model for lateral organ formation. *Front. Plant Sci.* **5**, 117 (2014).

550 3. Skinner, D. J., Hill, T. A. & Gasser, C. S. Regulation of Ovule Development.
551 *PLANT CELL ONLINE* **16**, S32–S45 (2004).

552 4. Smyth, D. R., Bowman, J. L. & Meyerowitz, E. M. Early Flower Development in
553 Arabidopsis. *Plant Cell* **2**, 755–767 (1990).

554 5. Alonso-Blanco, C., Blankestijn-de Vries, H., Hanhart, C. J. & Koornneef, M.
555 Natural allelic variation at seed size loci in relation to other life history traits of
556 Arabidopsis thaliana. *Proc. Natl. Acad. Sci. U. S. A.* **96**, 4710–7 (1999).

557 6. Cucinotta, M. *et al.* Cytokinin response factors integrate auxin and cytokinin
558 pathways for female reproductive organ development. *Development* **143**,
559 4419–4424 (2016).

560 7. Cucinotta, M. *et al.* CUP-SHAPED COTYLEDON1 (CUC1) and CUC2 regulate

561 cytokinin homeostasis to determine ovule number in Arabidopsis. *J. Exp. Bot.* **69**,
562 5169–5176 (2018).
563 8. Bencivenga, S., Simonini, S., Benkova, E. & Colombo, L. The Transcription
564 Factors BEL1 and SPL Are Required for Cytokinin and Auxin Signaling During
565 Ovule Development in Arabidopsis. *Plant Cell* **24**, 2886–2897 (2012).
566 9. Gomez, M. D. *et al*. Gibberellins negatively modulate ovule number in plants.
567 *Development* **145**, dev163865 (2018).
568 10. Galbiati, F. *et al.* An integrative model of the control of ovule primordia formation.
569 *Plant J.* **76**, 446–455 (2013).
570 11. Yuan, J. & Kessler, S. A. A genome-wide association study reveals a novel
571 regulator of ovule number and fertility in Arabidopsis thaliana. *PLOS Genet.* **15**,
572 e1007934 (2019).
573 12. Rédei, G. P. Single locus heterosis. *Z. Vererbungsl.* **93**, 164–170 (1962).
574 13. Torii, K. U. *et al*. The Arabidopsis ERECTA gene encodes a putative receptor
575 protein kinase with extracellular leucine-rich repeats. *Plant Cell* **8**, 735–746
576 (1996).

14. Shpak, E. D., McAbee, J. M., Pillitteri, L. J. & Torii, K. U. Stomatal Patterning and Differentiation by Synergistic Interactions of Receptor Kinases. *Science (80-.).* **309**, 290–293 (2005).

15. Shpak, E. D., Berthiaume, C. T., Hill, E. & Torii, K. U. Synergistic interaction of three ERECTA-family receptor-like kinases controls Arabidopsis organ growth and flower development by promoting cell proliferation. *Development* **131**, 1491–1501 (2004).

16. Uchida, N. & Tasaka, M. Regulation of plant vascular stem cells by endodermis-derived EPFL-family peptide hormones and phloem-expressed ERECTA-family receptor kinases. *J. Exp. Bot.* **64**, 5335–5343 (2013).

17. Tameshige, T. *et al.* A Secreted Peptide and Its Receptors Shape the Auxin Response Pattern and Leaf Margin Morphogenesis. *Curr. Biol.* **26**, 2478–2485 (2016).

18. Hara, K. *et al.* Epidermal Cell Density is Autoregulated via a Secretory Peptide, EPIDERMAL PATTERNING FACTOR 2 in Arabidopsis Leaves. *Plant Cell Physiol.* **50**, 1019–1031 (2009).

593 19. Hara, K., Kajita, R., Torii, K. U., Bergmann, D. C. & Kakimoto, T. The secretory
594 peptide gene EPF1 enforces the stomatal one-cell-spacing rule. *Genes &*
595 *jinDevelopment* **21**, 1720–1725 (2007).
596 20. Hunt, L. & Gray, J. E. The Signaling Peptide EPF2 Controls Asymmetric Cell
597 Divisions during Stomatal Development. *Curr. Biol.* **19**, 864–869 (2009).
598 21. Sugano, S. S. *et al.* Stomagen positively regulates stomatal density in Arabidopsis.
599 *Nature* **463**, 241–244 (2010).
600 22. Kondo, T. *et al.* Stomatal density is controlled by a mesophyll-derived signaling
601 molecule. *Plant Cell Physiol.* **51**, 1–8 (2010).
602 23. Hunt, L., Bailey, K. J. & Gray, J. E. The signalling peptide EPFL9 is a positive
603 regulator of stomatal development. *New Phytol.* **186**, 609–614 (2010).
604 24. Lee, J. S. *et al.* Direct interaction of ligand-receptor pairs specifying stomatal
605 patterning. *Genes Dev.* **26**, 126–136 (2012).
606 25. Lee, J. S. *et al.* Competitive binding of antagonistic peptides fine-tunes stomatal
607 patterning. *Nature* **522**, 439–443 (2015).
608 26. Qi, X. *et al.* Autocrine regulation of stomatal differentiation potential by EPF1 and

609 ERECTA-LIKE1 ligand-receptor signaling. *Elife* **6**, 1–21 (2017).

610 27. Davies, K. A. & Bergmann, D. C. Functional specialization of stomatal bHLHs

611 through modification of DNA-binding and phosphoregulation potential. *Proc.*

612 *Natl. Acad. Sci.* **111**, 15585–15590 (2014).

613 28. Lampard, G. R., MacAlister, C. A. & Bergmann, D. C. Arabidopsis Stomatal

614 Initiation Is Controlled by MAPK-Mediated Regulation of the bHLH

615 SPEECHLESS. *Science (80-.).* **322**, 1113–1116 (2008).

616 29. Koornneef, M., Alonso-Blanco, C. & Vreugdenhil, D. Naturally occurring genetic

617 variation in Arabidopsis thaliana. *Annu. Rev. Plant Biol.* **55**, 141–172 (2004).

618 30. van Zanten, M. *et al.* Ethylene-induced hyponastic growth in Arabidopsis thaliana

619 is controlled by ERECTA. *Plant J.* **61**, 83–95 (2010).

620 31. Godiard, L. *et al.* ERECTA, an LRR receptor-like kinase protein controlling

621 development pleiotropically affects resistance to bacterial wilt. *Plant J.* **36**,

622 353–365 (2003).

623 32. Bemis, S. M., Lee, J. S., Shpak, E. D. & Torii, K. U. Regulation of floral patterning

624 and organ identity by arabidopsis erecta-family receptor kinase genes. *J. Exp. Bot.*

(2013). doi:10.1093/jxb/ert270

33. Uchida, N. *et al.* Regulation of inflorescence architecture by intertissue layer ligand-receptor communication between endodermis and phloem. *Proc. Natl. Acad. Sci.* **109**, 6337–6342 (2012).

34. Abrash, E. B. & Bergmann, D. C. Regional specification of stomatal production by the putative ligand CHALLAH. *Development* **137**, 447–455 (2010).

35. Abrash, E. B., Davies, K. A. & Bergmann, D. C. Generation of Signaling Specificity in Arabidopsis by Spatially Restricted Buffering of Ligand–Receptor Interactions. *Plant Cell* **23**, 2864–2879 (2011).

36. Sahana, G., de Koning, D. J., Guldbrandtsen, B., Sørensen, P. & Lund, M. S. The efficiency of mapping of quantitative trait loci using cofactor analysis in half-sib design. *Genet. Sel. Evol.* **38**, 167–182 (2006).

37. Kirch, T., Simon, R., Grünewald, M. & Werr, W. The DORNRÖSCHEN/ENHANCER OF SHOOT REGENERATION1 Gene of Arabidopsis Acts in the Control of Meristem Cell Fate and Lateral Organ Development. *Plant Cell* **15**, 694–705 (2003).

641 38. Cole, M. *et al.* DORNRÖSCHEN is a direct target of the auxin response factor
642 MONOPTEROS in the Arabidopsis embryo. *Development* **136**, 1643–1651
643 (2009).
644 39. Liao, C. *et al.* Reporters for sensitive and quantitative measurement of auxin
645 response. *Nat. Methods* **12**, 207–210 (2015).
646 40. Pillitteri, L. J., Bemis, S. M., Shpak, E. D. & Torii, K. U. Haploinsufficiency after
647 successive loss of signaling reveals a role for ERECTA -family genes in
648 Arabidopsis ovule development. **3109**, 3099–3109 (2007).
649 41. Ho, C.-M. K., Paciorek, T., Abrash, E. & Bergmann, D. C. Modulators of Stomatal
650 Lineage Signal Transduction Alter Membrane Contact Sites and Reveal
651 Specialization among ERECTA Kinases. *Dev. Cell* **38**, 345–357 (2016).
652 42. Kurihara, D., Mizuta, Y., Sato, Y. & Higashiyama, T. ClearSee: a rapid optical
653 clearing reagent for whole-plant fluorescence imaging. *Development* 4168–4179
654 (2015). doi:10.1242/dev.127613
655 43. Yokoyama, R., Takahashi, T., Kato, A., Torii, K. U. & Komeda, Y. The
656 Arabidopsis ERECTA gene is expressed in the shoot apical meristem and organ

657 primordia. *Plant J.* **15**, 301–310 (1998).

658 44. Kosentka, P. Z., Overholt, A., Maradiaga, R., Mitoubsi, O. & Shpak, E. D. EPFL

659 Signals in the Boundary Region of the SAM Restrict Its Size and Promote Leaf

660 Initiation. *Plant Physiol.* **179**, 265–279 (2019).

661 45. Lin, G. *et al.* A receptor-like protein acts as a specificity switch for the regulation

662 of stomatal development. *Genes Dev.* **31**, 927–938 (2017).

663 46. Nadeau, J. A. & Sack, F. D. Control of Stomatal Distribution on the Arabidopsis

664 Leaf Surface. *Science (80-.).* **296**, 1697–1700 (2002).

665 47. Gonçalves, B. *et al.* A conserved role for CUP-SHAPED COTYLEDON genes

666 during ovule development. *Plant J.* **83**, 732–742 (2015).

667 48. Yano, K. *et al.* Genome-wide association study using whole-genome sequencing

668 rapidly identifies new genes influencing agronomic traits in rice. *Nat. Genet.*

669 (2016). doi:10.1038/ng.3596

670 49. Bessho-Uehara, K. *et al.* Loss of function at RAE2 , a previously unidentified

671 EPFL, is required for awnlessness in cultivated Asian rice . *Proc. Natl. Acad. Sci.*

672 (2016). doi:10.1073/pnas.1604849113

673 50. Jin, J. *et al.* GAD1 Encodes a Secreted Peptide That Regulates Grain Number,
674 Grain Length, and Awn Development in Rice Domestication . *Plant Cell* **28**,
675 2453–2463 (2016).
676 51. Zhang, Y. *et al.* Natural alleles of GLA for grain length and awn development
677 were differently domesticated in rice subspecies japonica and indica . *Plant*
678 *Biotechnol. J.* 1–13 (2019). doi:10.1111/pbi.13080
679 52. Nordborg, M. *et al.* The Pattern of Polymorphism in Arabidopsis thaliana. *PLoS*
680 *Biol.* **3**, e196 (2005).
681 53. Broman, K. W., Wu, H., Sen, S. & Churchill, G. A. R/qtl: QTL mapping in
682 experimental crosses. *Bioinformatics* **19**, 889–890 (2003).
683 54. Hahn, F. *et al.* An Efficient Visual Screen for CRISPR/Cas9 Activity in
684 Arabidopsis thaliana. *Front. Plant Sci.* **08**, (2017).
685 55. Lampropoulos, A. *et al.* GreenGate - A Novel , Versatile , and Efficient Cloning
686 System for Plant Transgenesis. **8**, (2013).
687 56. Kawamoto, N., Sasabe, M., Endo, M., Machida, Y. & Araki, T.
688 Calcium-dependent protein kinases responsible for the phosphorylation of a bZIP

689 transcription factor FD crucial for the florigen complex formation. *Sci. Rep.* **5**,
690 8341 (2015).

691

692 Figure legends

693 **Figure 1. Identification of responsible loci for the reproductive traits.** (A) Image of
694 seed density in L. *er* (left) and Cvi-0 (right). Bar = 1 mm. (B) Natural variation analysis
695 on seed density (seed number/fruit length (mm)) phenotype at 16˚C (cyan) and 21˚C (red).
696 Fourteen selected representative accessions are presented. See the supplementary figure 1
697 for the phenotype of all accessions. (C) QTL analysis using L. *er* x Cvi-0 recombinant
698 inbred lines [45]. (D) QTL re-analysis with ER as a cofactor. X and Y axes indicate
699 chromosome position and LOD values, respectively.

700

701 **Figure 2. Genetic and expression analysis of ER family receptors**
702 (A) Seed density (seed number/fruit length (mm)). 40 fruits were measured from 3 plants
703 in each genotype. (B) Two weeks old *er-105; erl1-2; erl2-1* plant. (C) Six weeks old
704 *er-105; erl1-2; erl2-1* plant. Expression patterns of ER, ERL1 and ERL2 in stage 8 flower

(D, F, H) or later stage (E, G, I) of developing pistils. se, st, ca, v and r indicate sepals, stamens, carpels, valve, replum, respectively. (D, F, H) and (E, G, I) share same scales, respectively. Scale bar = 1 mm (B), 5 mm (C) and 50 μm (D, E, F, G, H, I). Tukey-Kramer's test was used for the statistical analysis. Different letters indicate significant difference ($p < 0.005$).

Figure 3. Identification of EPFL9 as a potential ligand for ER

(A) Seed density (seed number/fruit length (mm)). 40 fruits were measured from 3 plants in each genotype. (B-E) Expression pattern of EPFL9 at stage 8 flower (B, C) and stage 9 flower (D, E). Transverse cross section (C, E) were obtained along the lines in (B) and (D). st, ca, v and r indicate sepals, stamens, carpels, valve, replum, respectively. Histone H2B fused EGFP was used as a reporter. Bar = 50 μm. Student's t-test was used for the statistical analysis. Different letters indicate significant difference ($p < 0.005$).

Figure 4. Identification of EPFL2 as a patterning regulator of ovule initiation

(A) Seed density (seed number/fruit length(mm)). 40 fruits were measured from 3 plants

721 in each genotype. (B) Genetic interaction analysis either with *er-105* or *erl1-2; erl2-1*.
722 (C-G) Expression patterns of EPFL2. Histone H2B fused TdTomato was used as a
723 reporter. Developing pistil in stage 8 flower (C, D), and stage 9 flower (E, F). (G) A
724 magnified view of a white box in (E). Transverse cross section (D, F) were obtained along
725 the lines. v and r indicate valve and replum, respectively. Bar = 100 μm. Student's t-test
726 was used for the statistical analyses (A) and Tukey-Kramer's test was used for the
727 statistical analyses (C, D). Different letters indicate significant difference ($p < 0.005$).
728
729 **Figure 5. Disrupted regular patterning in ovule spacing in *epfl2* and ectopic**
730 **expression of EPFL2**
731 (A, B) Ovule twinning phenotype in *epfl2-2*. (C-E) R2D2 expression in developing ovule
732 primordia. Arrow heads indicate auxin maxima. (F, G) Expression pattern of *DRN* before
733 acquiring ovule identity. (H, I) Expression pattern of *DRN* after arising ovule primordia.
734 (J) Initiation of ovule primordia in wild-type (*pDRN::GFP*; Col) plants and (K) *epfl2*
735 mutant (*pDRN::GFP*; *epfl2-2*) plants. (L) Quantification of cell number between ovule
736 initial cells. Counted cells were indicated by dots in (J) and (K) as an example. F-test was

737 used for the statistical analysis. (M) Seed density (seed number/fruit length (mm))
738 phenotype in *pDRN::EPFL2*; Col transgenic plants. Student's t-test was used for the
739 statistical analysis. Different letters indicate significant difference ($p < 0.005$). Scale bar =
740 500 μm (A, B), 50 μm (C, D, E, F, H), 20 μm (J, K).
741
742 **Figure 6. Coordination of fruit growth and ovule patterning by two**
743 **peptide-receptor pairs**
744 (A) Graphical summary of expression patterns of EPFL2 (magenta) and EPFL9 (yellow).
745 (B) Two pathways control ovule initiation pattern and fruit growth to archive coordinated
746 fruit growth. (C) The interaction between EPFL2 (magenta) and auxin (green) establishes
747 regular ovule pattern in placenta.
748 **Supplementary Figures**
749 **Figure S1. Natural variation analysis on fruit length and seed number**
750 96 Arabidopsis thaliana natural accessions were analyzed on fruit length and seed number
751 per fruit at 16˚C and 21˚C. Each point indicates average values of fruit length and seed
752 number. Acccessions in red points are presented in Figure 1B.

753

754 **Figure S2. Complementation of L. er, Van-0 and Hir-1 by functional ER genomic**

755 **sequence**

756 (A) Fruit length phenotype. (B) Seed number per fruit. (C) Seed density. Student's t-test

757 was used for the statistical analyses. Different letters indicate significant difference (p<

758 0.005).

759

760 **Figure S3. Fruit length and seed number in ER family receptor mutants**

761 (A) Fruit length (mm) and (B) seed number per fruit were analyzed in Columbia

762 background mutants. Tukey-Kramer's test was used for the statistical analyses. Different

763 letters indicate significant difference (p< 0.005).

764

765 **Figure S4. Fruit phenotype of STOMAGEN RNAi plants**

766 (A) Fruit length (mm) and (B) seed number per fruit were analyzed. STOMAGEN RNAi

767 plants were generated [17]. Student's t-test was used for the statistical analyses. Different

768 letters indicate significant difference (p< 0.005).

769

770 **Figure S5. Genetic interaction analysis between *er* and *epfl2* in Landsberg**

771 (A) Fruit length (mm) and (B) seed number per fruit were analyzed in Landsberg

772 background mutants. L. *er ER*+ was used as for wild-type plants. Tukey-Kramer's test

773 was used for the statistical analyses. Different letters indicate significant difference ($p <$

774 0.005).

775

776 **Figure S6. Generation of *epfl2* knockout mutant in Col background by**

777 **CRISPR/Cas9**

778 (A) Design of sgRNA. Boxes and lines indicate exons and introns, respectively. Green

779 and white boxes indicate coding regions corresponding to mature peptide and 3'

780 untranslated region (UTR), respectively. Arrowheads indicate the position of sgRNA1

781 and sgRNA2. (B) Sequences of newly isolated *epfl2* mutant alleles. Black bars indicate

782 the positions of sgRNA and red bars indicate the positions of protospacer adjacent motif

783 (PAM), respectively. (C) Leaf margin phenotype of *epfl2* mutant alleles. Seventh true

784 leaves were photographed according to [13]. Scale bars = 1 cm.

785

786 **Figure S7. Fruit phenotype of *epfl2* mutants**

787 (A) Fruit length (mm) and (B) seed number per fruit were analyzed. Student's t-test was

788 used for the statistical analyses. Different letters indicate significant difference (p<

789 0.005).

790

791 **Figure S8. Genetic analysis of *epfl2* and ER family receptors: Fruit length and seed**

792 **number phenotypes**

793 Double mutant analysis of *epfl2-2; er-105* in fruit length (A) and seed number per fruit

794 (B). Triple mutant analysis of *epfl2-2; erl1-2; erl2-1* in fruit length (C) and seed number

795 per fruit (D). Tukey-Kramer's test was used for the statistical analyses. Different letters

796 indicate significant difference (p< 0.005).

797

798 **Figure S9. Fruit phenotype of *pDRN::EPFL2* plants**

799 (A) Fruit length (mm) and (B) seed number per fruit were analysed. Student's t-test was

800 used for the statistical analyses. Different letters indicate significant difference (p<

0.005).

Figure S10. Expression pattern of *TMM*

pTMM::GUS expression in stage 5-10 flower buds (A), stage 11 flower (B) and stage 12 flower (C). Scale bar = 2 mm.

Figure S11. Evaluation of recombinant peptide bioactivity based on stomatal density

Representative images of epidermis after peptides and mock treatments in wild-type (A-D) and *tmm-KO* mutant (E-H). Scale bar = 100 μm. (I) Quantification of stomatal number per 0.2 mm^2. Each treatment were compared to mock treatment. Dunnett's test was used for the statistical analyses. A value of $p < 0.005$ was considered as significant.

Figure S12. Quantitative interaction analyses between EPFLs and ER-family receptors by using ITC

Isothermal titration calorimetry of the ERECTA family receptor domains with EPFL2

(A-C) and EPFL9 (D-F). 18 injections of 2µL of peptide (50 µM) were titrated into 280 µL of the receptor domain (5 µM) at a stirring rate of 750 rpm. The experiment was performed at 25°C. The thermograms show the detected peaks of the heat change after each injection (upper panel), the integrated values were subjected to either the "one binding site" (A-E) fitting algorithm of the Microcal ITC-ORIGIN software, or the "two binding sites" algorithm (F). Each square represents the integrated value of the corresponding peak and the line resembles the yielded fitting curve after chi^2 minimization (lower panel). The table lists the calculated *Kd* values for each interaction with the theoretical stoichiometry (G).

Supplemental Movie 1. Expression pattern of EPFL2 using two photon microscopy.

A z series of stage 9-10 pistil expressing H2B:TdTomato under the control of EPFL2 promoter. Images were acquired with 1 µm intervals by using two photon microscopy (Nikon A1R) with 1000 nm excitation.

Supplemental Movie 2. Expression pattern of EPFL2 using ClearSee and confocal microscopy.

A z series of ClearSee treated stage 9-10 pistil expressing H2B:TdTomato under the control of EPFL2 promoter. Images were acquired with 1 µm intervals by LSM880 with 561 nm excitation.

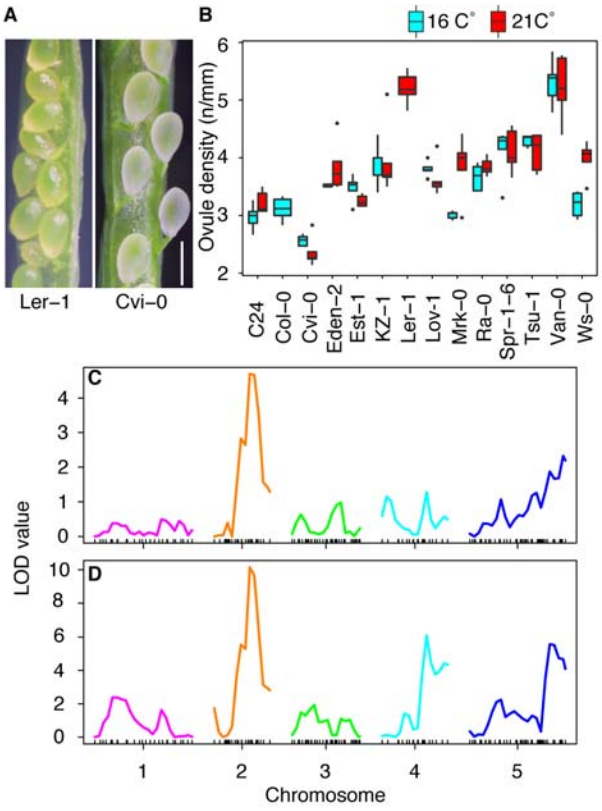

Figure 1. Identification of responsible loci for the reproductive traits. (A) Image of seed density in L. *er* (left) and Cvi-0 (right). Bar = 1 mm. (B) Natural variation analysis on seed density (seed number/fruit length (mm)) phenotype at 16˚C (cyan) and 21˚C (red). Fourteen selected representative accessions are presented. See the supplementary figure 1 for the phenotype of all accessions. (C) QTL analysis using L. *er* x Cvi-0 recombinant inbred lines [45]. (D) QTL re-analysis with ER as a cofactor. X and Y axes indicate chromosome position and LOD values, respectively.

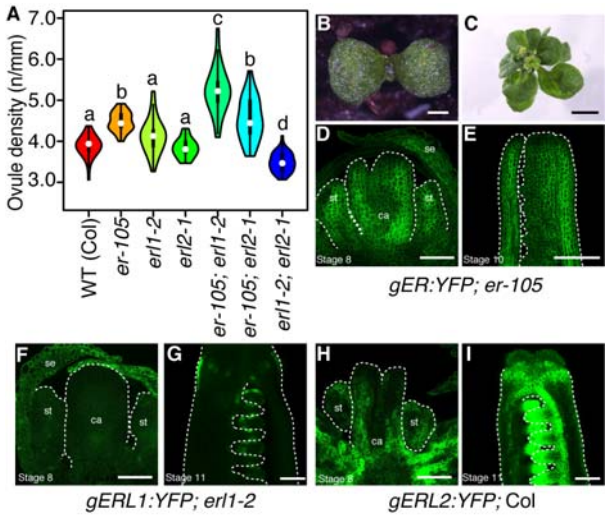

Figure 2. Genetic and expression analysis of ER family receptors

(A) Seed density (seed number/fruit length (mm)). 40 fruits were measured from 3 plants in each genotype. (B) Two weeks old *er-105; erl1-2; erl2-1* plant. (C) Six weeks old *er-105; erl1-2; erl2-1* plant. Expression patterns of ER, ERL1 and ERL2 in stage 8 flower (D, F, H) or later stage (E, G, I) of developing pistils. se, st, ca, v and r indicate sepals, stamens, carpels, valve, replum, respectively. (D, F, H) and (E, G, I) share same scales, respectively. Scale bar = 1 mm (B), 5 mm (C) and 50 μm (D, E, F, G, H, I). Tukey-Kramer's test was used for the statistical analysis. Different letters indicate significant difference ($p < 0.005$).

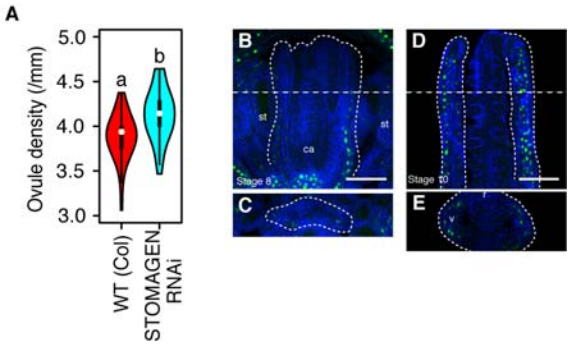

Figure 3. Identification of EPFL9 as a potential ligand for ER

(A) Seed density (seed number/fruit length (mm)). 40 fruits were measured from 3 plants in each genotype. (B-E) Expression pattern of EPFL9 at stage 8 flower (B, C) and stage 9 flower (D, E). Transverse cross section (C, E) were obtained along the lines in (B) and (D). st, ca, v and r indicate sepals, stamens, carpels, valve, replum, respectively. Histone H2B fused EGFP was used as a reporter. Bar = 50 μm. Student's t-test was used for the statistical analysis. Different letters indicate significant difference ($p < 0.005$).

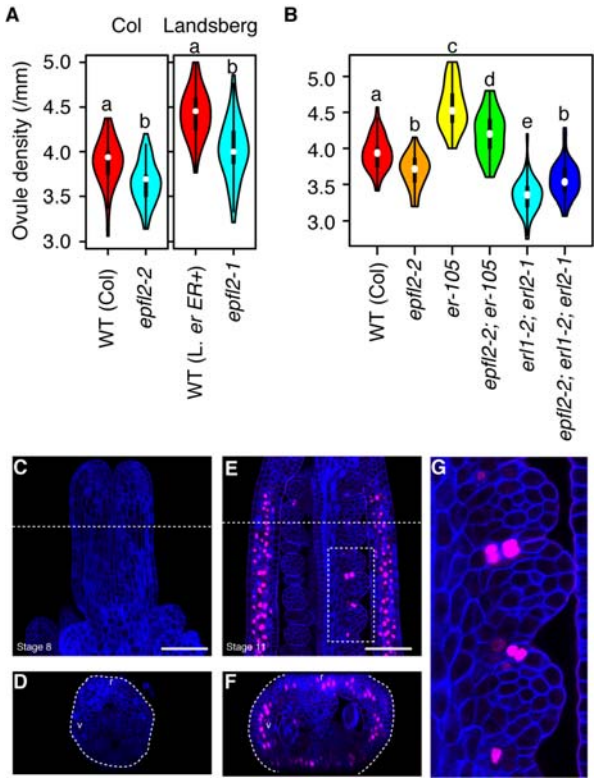

Figure 4. Identification of EPFL2 as a patterning regulator of ovule initiation

(A) Seed density (seed number/fruit length(mm)). 40 fruits were measured from 3 plants in each genotype. (B) Genetic interaction analysis either with *er-105* or *erl1-2; erl2-1*. (C-G) Expression patterns of EPFL2. Histone H2B fused TdTomato was used as a reporter. Developing pistil in stage 8 flower (C, D), and stage 9 flower (E, F). (G) A magnified view of a white box in (E). Transverse cross section (D, F) were obtained along the lines. v and r indicate valve and replum, respectively. Bar = 100 μm. Student's t-test was used for the statistical analyses (A) and Tukey-Kramer's test was used for the statistical analyses (C, D). Different letters indicate significant difference ($p < 0.005$).

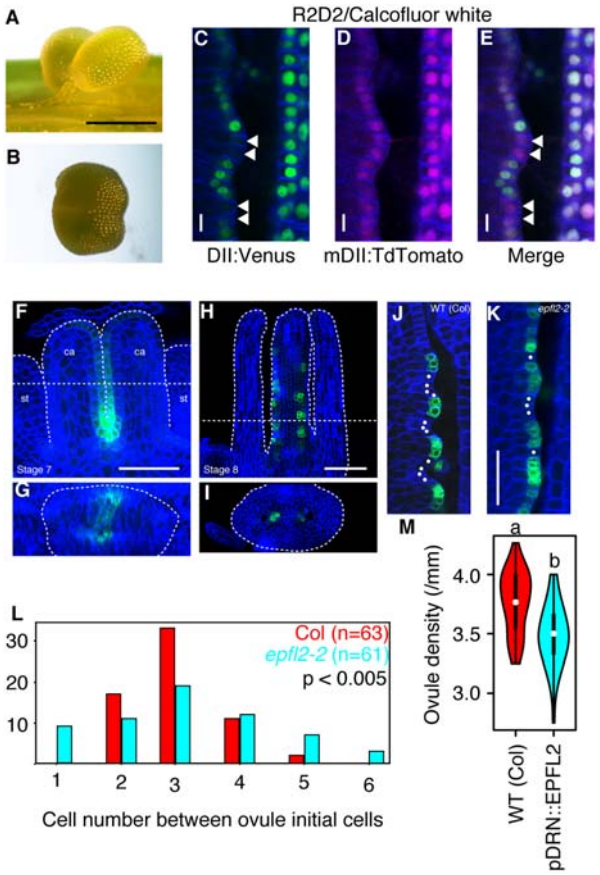

Figure 5. Disrupted regular patterning in ovule spacing in *epfl2* and ectopic expression of EPFL2

(A, B) Ovule twinning phenotype in *epfl2-2*. (C-E) R2D2 expression in developing ovule primordia. Arrow heads indicate auxin maxima. (F, G) Expression pattern of *DRN* before acquiring ovule identity. (H, I) Expression pattern of *DRN* after arising ovule primordia. (J) Initiation of ovule primordia in wild-type (*pDRN::GFP*; Col) plants and (K) *epfl2* mutant (*pDRN::GFP*; *epfl2-2*) plants. (L) Quantification of cell number between ovule initial cells. Counted cells were indicated by dots in (J) and (K) as an example. F-test was used for the statistical analysis. (M) Seed density (seed number/fruit length (mm)) phenotype in *pDRN::EPFL2*; Col transgenic plants. Student's t-test was used for the

statistical analysis. Different letters indicate significant difference ($p < 0.005$). Scale bar = 500 µm (A, B), 50 µm (C, D, E, F, H), 20 µm (J, K).

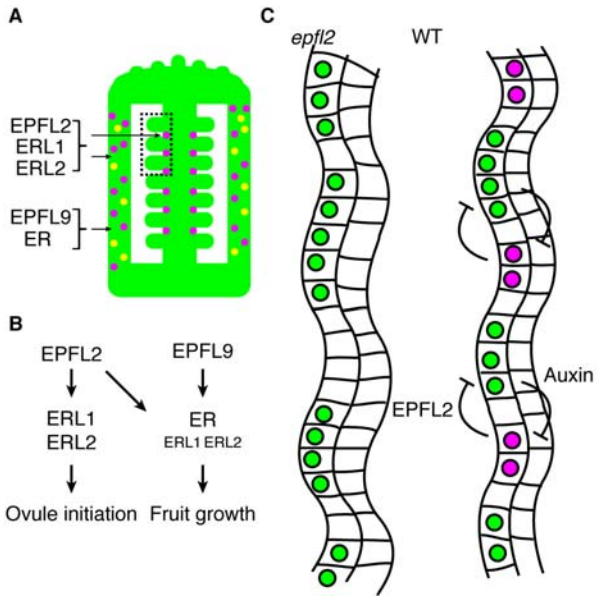

Figure 6. Coordination of fruit growth and ovule patterning by two peptide-receptor pairs

(A) Graphical summary of expression patterns of EPFL2 (magenta) and EPFL9 (yellow). (B) Two pathways control ovule initiation pattern and fruit growth to archive coordinated fruit growth. (C) The interaction between EPFL2 (magenta) and auxin (green) establishes regular ovule pattern in placenta.